



Uni-DAD: Unified Distillation and Adaptation of Diffusion Models for Few-step Few-shot Image Generation

Yara Bahram*, Melodie Desbos*, Mohammadhadi Shateri, Eric Granger
 LIVIA, Dept. of Systems Engineering, ETS Montreal, Canada
 {yara.mohammadi-bahram, melodie.desbos}@olivia.etsmtl.ca,
 {mohammadhadi.shateri, eric.granger}@etsmtl.ca

Abstract

Diffusion models (DMs) produce high-quality images, yet their sampling remains costly when adapted to new domains. Distilled DMs are faster but typically remain confined within their teacher’s domain. Thus, fast and high-quality generation for novel domains relies on two-stage training pipelines: Adapt-then-Distill or Distill-then-Adapt. However, both add design complexity and suffer from degraded quality or diversity. We introduce Uni-DAD, a single-stage pipeline that unifies distillation and adaptation of DMs. It couples two signals during training: (i) a dual-domain distribution-matching distillation objective that guides the student toward the distributions of the source teacher and a target teacher, and (ii) a multi-head generative adversarial network (GAN) loss that encourages target realism across multiple feature scales. The source domain distillation preserves diverse source knowledge, while the multi-head GAN stabilizes training and reduces overfitting, especially in few-shot regimes. The inclusion of a target teacher facilitates adaptation to more structurally distant domains. We perform evaluations¹ on a variety of datasets for few-shot image generation (FSIG). Uni-DAD delivers higher quality than state-of-the-art (SoTA) adaptation methods even with ≤ 4 sampling steps, and outperforms two-stage training pipelines in both quality and diversity.

1. Introduction

DMs [14, 41, 43] have emerged as the dominant paradigm for generative modeling, achieving SoTA performance in image synthesis [8] and text-to-image generation [34, 36]. These models produce high-quality and diverse images even when adapted to novel domains and subjects, given only

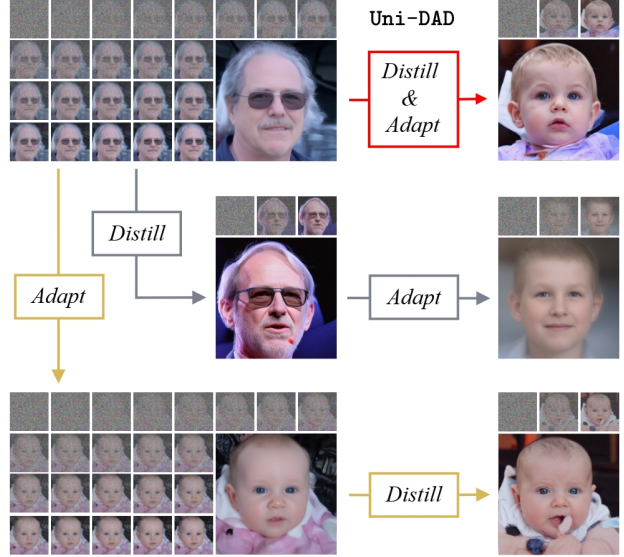


Figure 1. **Uni-DAD** (*Distill & Adapt*) vs. two-stage pipelines, **Distill-then-Adapt**, and **Adapt-then-Distill**. *Adapt* is performed by fine-tuning, and *Distill* by DMD2 [49]. The source domain is represented by 70K diverse faces, and the target domain by 10 babies. Sampling steps are reduced from 25 to 3.

a handful of images. This makes them an attractive solution for FSIG [3, 52] and subject-driven personalization (SDP) [9, 19, 35]. However, DMs need an iterative denoising procedure over many time-steps for sampling, resulting in slow test-time generation. Adapted models inherit this cost, challenging real-time personalized use-cases. Distillation alleviates the slow inference by training a few-step student to mimic a larger teacher DM [5, 37, 44, 49, 50]. Ultimately, the ability to generate images in novel domains in few-shot contexts while requiring only a few denoising steps can facilitate the deployment of DMs in personalized real-time applications.

*Equal contribution

¹Our code is included in suppl. materials and will be made public.

In recent works, reducing the number of time-steps and adapting to new domains requires a two-stage pipeline: *Distill-then-Adapt* or *Adapt-then-Distill*. The former is more compute-friendly as a student can be adapted per task after a single compute-heavy distillation step. Yet, students often saturate their adaptation capacity, yielding over-smoothed outputs on few-shot target domains [27]. Further, fine-tuning a student under the teacher’s original diffusion loss negates the benefits of distillation [27]. *Adapt-then-Distill* can yield higher image quality and mitigate over-smoothing. However, the student remains tied to the adapted teacher’s performance and is prone to overfitting. Conversely, neither of the two-stage pipelines is an end-to-end process, and both are susceptible to losing diverse transferable source information during the training processes.

We propose Unified Distillation and Adaptation of Diffusion models (Uni-DAD), a single-stage pipeline that compresses a high-quality DM teacher into a few-step student, while adapting it to a few-shot target domain (Fig. 1). It couples two complementary signals: a dual-domain distribution-matching distillation (DMD) objective and a multi-head GAN loss. The dual-domain DMD guides the student’s generation with the scores of a frozen source-domain teacher and optionally an online target-domain teacher. The inclusion of the target teacher improves adaptation to structurally distant domains. This dual-domain design guides the student toward a common area between the two distributions while preserving source diversity. The multi-head GAN enforces target realism across multiple feature scales, reducing overfitting in few-shot regimes. An online fake teacher tracks the evolving student distribution and provides up-to-date negatives for the discriminator in the GAN framework. Uni-DAD training iterates among updating (i) the student, (ii) the online fake teacher and discriminator, and optionally (iii) an online target teacher. These objectives allow the student to preserve source-derived diversity while sharpening target realism. The end result is a few-step generator that produces diverse high-quality images of a novel domain in few-shot contexts. Uni-DAD is checkpoint-agnostic: a pre-adapted target DM can replace the online target teacher with no additional training needed, and a pre-distilled source DM can initialize the student. As a result, our method enables distillation of adapted models and adaptation of distilled models without any changes to the training loop.

Uni-DAD is extensively validated on four target sets with varying levels of source proximity on the task of FSIG [28] with guided denoising diffusion probabilistic model (DDPM) [8]. It attains higher quality with substantially fewer sampling steps than related SoTA adaptation methods and outperforms two-stage pipelines in terms of quality and diversity. Our single-step pipeline offers a practical path to fast personalized image generation.

Contributions. (i) This paper introduces the first single-stage pipeline that jointly distills and adapts a DM for fast, high-quality, and diverse generation in novel domains. (ii) Dual-domain DMD and multi-head GAN losses are proposed to help retain source-domain diversity while sharpening target domain realism under few-shot data. An optional target teacher facilitates adaptation to structurally distant domains. (iii) On FSIG benchmarks, our method achieves higher quality with substantially fewer sampling steps than prior non-distilled adaptation methods and outperforms two-stage pipelines in quality and diversity.

2. Related Work

(a) Diffusion Distillation. To address the costly DM inference, efficient numerical solvers such as DDIM [42] and DPM-Solver [21] allow compressing the long denoising trajectory without retraining the DM (neural function evaluations, NFE ~ 10). Knowledge distillation, on the other hand, trains a few-step student generator to mimic a teacher DM ($1 \leq \text{NFE} \leq 4$). Progressive distillation halves steps by matching the teacher across adjacent time-steps [37]. Consistency-based methods directly learn a one-step mapping from noise to data [22, 44]. Recently, by combining score distillation with adversarial training, DMD [49, 50], ADD [38, 39], and FlashDiffusion [5], yield few-step students that match or surpass their teacher in quality. However, the students remain tied to the teacher’s manifold, limiting flexibility under domain shift. Furthermore, the adversarial objective assumes access to large training corpora that is unavailable in few-shot applications, where the GAN’s discriminator easily memorizes the target set. We focus on distillation in the face of domain-shift and few-shot target sets.

(b) Diffusion Adaptation. Adaptation involves updating a model pretrained on a large source domain to fit a related, smaller target domain. While naïve finetuning is standard for style transfer with ample data (target size $n \sim 1000$) [16], it easily leads to overfitting and diversity degradation in few-shot regimes ($n \leq 10$). This has motivated methods tailored to few-shot applications that preserve source-domain diversity [3, 35]. FSIG aims to synthesize diverse, high-quality samples from an unconditional target domain. Early progress included GAN-based approaches like cross-domain correspondance (CDC) [28], RiCK [51], and GenDA [47]. Diffusion-based FSIG has become prominent for its quality: pairwise adaptation (DDPM-PA) applies CDC-style regularization [52] and conditional diffusion relaxing inversion (CRDI) learns a sample-wise guidance without base-model fine-tuning [3]. In both cases, however, sampling remains slow, leaving diffusion-based FSIG substantially slower than GANs. This paper instead focuses on fast sampling while preserving diversity and generation quality in both applications.

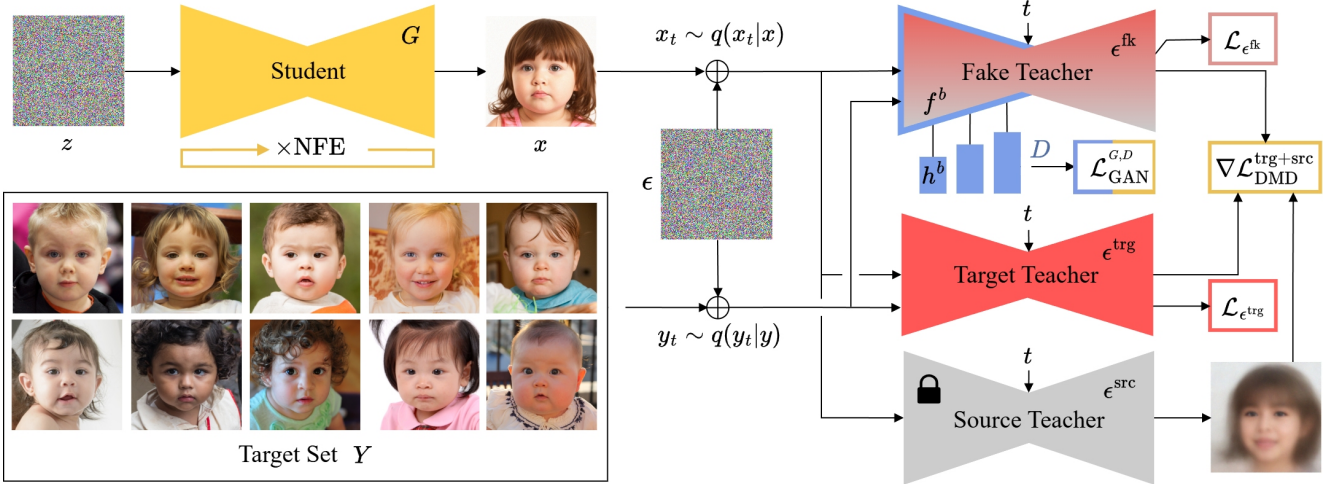


Figure 2. Overview of Uni-DAD for few-step and few-shot image generation. A (frozen) ϵ^{src} is adapted and distilled into a **student** G for fast sampling ($1 \leq \text{NFEs} \leq 4$) on the target domain. At each training iteration, Uni-DAD alternates among three updates: (1) **Student**: optimize G with a dual-domain DMD objective on ϵ^{src} and **target teacher** ϵ^{trg} , plus a GAN generator loss; (2) **Fake teacher and discriminator**: train a **fake teacher** ϵ^{fk} on student generations and train a **multi-head discriminator** D to distinguish target images from student generations; (3) **Target teacher update**: train ϵ^{trg} on target images.

(c) Combining Adaptation and Distillation. Transforming a large source-domain model to a smaller target domain one is commonly staged as *Adapt-then-Distill*, *Distill-then-Adapt*, or *Distill and Adapt* [48]. Below, we provide an analysis for each pipeline through the lens of DMs.

- *Distill-then-Adapt*: A one-time distillation followed by downstream adaptation is attractive for efficiency, as distillation is typically more costly than adaptation. However, prior work suggests that students often saturate in adaptation capacity. Specifically, naïvely fine-tuning the student with the original diffusion loss negates the benefits of distillation, yielding blurry, low-detail samples [27] (Fig. 1, middle). PSO [27] trains the student with a relative likelihood objective, alleviating the blur under lightweight style transfer in larger data regimes ($n \sim 1000$). However, output remains over-smoothed in few-shot contexts such as SDP. Several distillation methods emphasize producing students that remain LoRA-friendly after distillation [5, 23, 49]. However, LoRA-adapted models lag full finetuning under stronger distribution shifts and few-shot data.

- *Adapt-then-Distill*: Adapting the teacher to the target domain before distillation can mitigate the over-smoothed generations observed in *Distill-then-Adapt* pipelines. Moreover, a GAN objective during the distillation can potentially alleviate source-domain leakage and inconsistent fitting of a fine-tuned teacher [45] (Tab. 5). However, distillation on few-shot target data remains highly prone to overfitting (Sec. 2-b). Further, the student loses access to transferable source information and its generation quality remains

tied to the adapted teacher, inheriting any mis-adaptation.

- *Distill and Adapt*: To our knowledge, no prior work performs single-stage distillation and adaptation of DMs. Codi [25] comes close to our task. It jointly adapts an unconditional teacher to image-conditioned tasks (inpainting and super-resolution) while distilling it to a few-step student. Its focus, however, is on providing image control within the teacher manifold rather than few-shot adaptation to off-manifold target domains. A complementary line distills classifier-free guidance [13]. Plug-and-play guidance distillation learns a modular guidance head that can be connected to adapted models [15], while DogFit integrates guidance distillation into transfer learning [2]. These approaches reduce NFE in half by removing the two-step cost of guidance, but do not reduce the *number of denoising steps*, which is the focus of this paper.

3. Proposed Method

3.1. Background on DMs

DDPMs [14, 41, 43] are generative models that learn to reverse a fixed noising process applied over T time-steps. Starting from a clean image x , noise ϵ is gradually added to produce a sequence of noisy images $\{x_t\}_{t=1}^T$ where $x_t \sim q(x_t | x) = \mathcal{N}(\alpha_t x, \sigma_t^2 I)$ with α_t and σ_t controlling the noise schedule. A neural network $\epsilon(x_t, t)$ with parameters π is trained to predict ϵ at each t , using a mean squared error



Figure 3. Sensitivity analysis of sample quality to NFE.

(MSE) objective:

$$\mathcal{L}(\pi) = \mathbb{E}_{t,x,\epsilon} \left[\omega_t \|\epsilon_\pi(x_t, t) - \epsilon\|^2 \right], \quad (1)$$

where $\omega_t > 0$ is determined by the noise schedule. In subsequent equations, t and π are omitted when clear from context. In conditional generation, the model receives an auxiliary input c (e.g., class labels or text prompts), producing $\epsilon(x_t|c)$. SoTA DMs such as Stable Diffusion (SD) [29, 34] operate in the latent rather than pixel space.

3.2. Unified Adaptation and Distillation of DMs

Uni-DAD is proposed to compress a frozen source teacher DM ϵ^{src} trained with many time-steps ($T \sim 1000$) on a large source distribution $p^{\text{src}}(x)$ into a fast student generator G with parameters θ ($1 \leq \text{NFE} \leq 4$) while adapting to a target distribution $p^{\text{trg}}(y)$ represented by a few-shot target set Y ($|Y| \leq 10$). It couples two complementary signals for training G : (i) a dual-domain DMD against ϵ^{src} and optionally an online target teacher ϵ^{trg} , plus (ii) a multi-head GAN loss encouraging target realism across multiple feature scales. A fake teacher ϵ^{fk} is maintained to track the evolving student distribution, and attach a multi-head discriminator D to distinguish the student generations from Y . Additionally, a ϵ^{trg} can be fine-tuned on Y to further improve in matching the target distribution. The training alternates among optimizing the three models, G , $\epsilon^{\text{fk}} + D$, and optionally ϵ^{trg} (Fig. 2).

The next subsections detail each component: dual-domain DMD (Sec. 3.3), fake and target teachers (Sec. 3.4), and multi-head GAN (Sec. 3.5), while Sec. 3.6 describes the integration of components and overall training objective.

3.3. Dual-domain DMD

DMD is originally used to align a student’s distribution p^{fk} to p^{src} within the source domain [49, 50]. It minimizes KL-divergence of the two distributions at the current student outputs, nudging the student generator toward higher density regions of p^{src} . Computing the probability densities to estimate the loss $\mathcal{L}_{\text{DMD}}(\theta)$ is generally intractable [50]. However, the gradient of this loss with respect to θ can be obtained:

$$\begin{aligned} \nabla_\theta \mathcal{L}_{\text{DMD}} &= \nabla_\theta D_{\text{KL}}(p^{\text{fk}} \| p^{\text{src}}) \\ &= \mathbb{E}_z \left[(\nabla_x \log p^{\text{fk}}(x) - \nabla_x \log p^{\text{src}}(x)) \frac{dG_\theta}{d\theta} \right], \end{aligned} \quad (2)$$

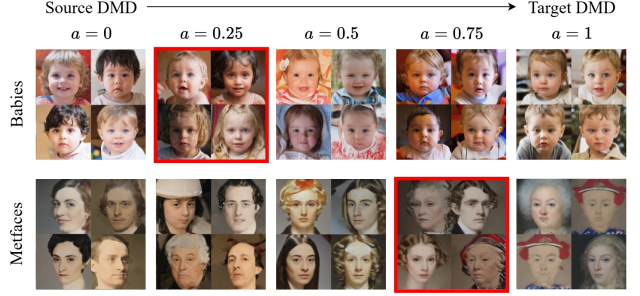


Figure 4. Qualitative ablation of the dual-domain DMD weighting factor a on Babies and MetFaces.

where $x = G(z)$, $z \sim \mathcal{N}(0, I)$ denotes the student output. Under Gaussian perturbation, the score satisfies $s(x_t) = \nabla_{x_t} \log p(x_t) = -\frac{1}{\sigma_t} \epsilon(x_t)$ [43]. Therefore, the right-hand terms of Eq. 2 can be approximated via two DMs: ϵ^{src} , and ϵ^{fk} , where ϵ^{src} is frozen and ϵ^{fk} is concurrently trained to track the evolving student outputs (Sec. 3.4). In practice, \mathcal{L}_{DMD} can be minimized by updating $\theta \leftarrow \theta - \eta \nabla_\theta \mathcal{L}_{\text{DMD}}$ with gradient descent.

We extend this formula to align the student outputs to both p^{src} and p^{trg} . The gradients of the two DMD losses can be written in noise-estimation form:

$$\begin{aligned} \nabla_\theta \mathcal{L}_{\text{DMD}^{\text{src}}} &\approx \mathbb{E}_{t,z} \left[\omega_t (\epsilon^{\text{fk}}(x_t) - \epsilon^{\text{src}}(x_t)) \frac{dG_\theta}{d\theta} \right], \\ \nabla_\theta \mathcal{L}_{\text{DMD}^{\text{trg}}} &\approx \mathbb{E}_{t,z} \left[\omega_t (\epsilon^{\text{fk}}(x_t) - \epsilon^{\text{trg}}(x_t)) \frac{dG_\theta}{d\theta} \right], \end{aligned} \quad (3)$$

where $t \sim \mathcal{U}\{0.02T, 0.98T\}$ and extreme time-steps are excluded for numerical stability [30]. We use a normalization that balances contributions across time-steps:

$$\omega_t = \frac{\sigma_t \cdot H \cdot S}{\|\epsilon - \epsilon^{\text{fk}}(x_t)\|_1}, \quad (4)$$

with H channels and S spatial locations [50]. Optimizing $\mathcal{L}_{\text{DMD}}^{\text{src}}$ can help retain diverse transferable information (e.g., pose, background, and facial expression), thereby compensating for target data scarcity. This objective suffices for adaptation in the face of small domain shifts. However, more structurally dissimilar target domains may contain regions outside the source manifold, in which case $\mathcal{L}_{\text{DMD}}^{\text{src}}$ can hold back true adaptation. A dual-domain DMD objective can guide the student toward a common area between the two distributions:

$$\nabla_\theta \mathcal{L}_{\text{DMD}}^{\text{trg+src}} = (1 - a) \nabla_\theta \mathcal{L}_{\text{DMD}^{\text{src}}} + a \nabla_\theta \mathcal{L}_{\text{DMD}^{\text{trg}}}, \quad (5)$$

where $a \in [0, 1]$ indicates a weighting factor, controlling the influence of each domain (Fig. 4).

3.4. Fake and Target Teachers

We initialize ϵ^{fk} with the weights of ϵ^{src} and update its parameters ϕ on the evolving student outputs by minimizing the MSE objective:

$$\mathcal{L}_{\text{fk}}(\phi) = \mathbb{E}_{t,z} \left[\left\| \epsilon_{\phi}^{\text{fk}}(x_t) - \epsilon \right\|_2^2 \right]. \quad (6)$$

During ϵ^{fk} updates, no gradients are propagated through G and x is treated as a fixed input. Similarly, ϵ^{trg} is initialized with the weights of ϵ^{src} and its parameters η are updated via the MSE to denoise diffused samples from Y via:

$$\mathcal{L}_{\text{trg}}(\eta) = \mathbb{E}_{t,\epsilon,y} \left[\left\| \epsilon_{\eta}^{\text{trg}}(y_t) - \epsilon \right\|_2^2 \right]. \quad (7)$$

The training and inclusion of ϵ^{trg} is optional in Uni-DAD, as it can facilitate adaptation of structure in face of strong domain shifts (see component ablations in Tab. 2). Further, if a pre-adapted ϵ^{trg} checkpoint is already available, it can be used as a fixed target teacher in the Uni-DAD algorithm without further training (see Tab. 3).

3.5. Multi-head GAN

To enforce sharp fidelity of student outputs to Y and stabilize the training, we use a multi-head GAN objective that judges target realism at multiple feature levels. While G plays the role of generator, the discriminator D reuses ϵ^{fake} encoder and middle blocks for feature extraction: let $f^b(\cdot)$ denote the feature extractor at block $b \in \mathcal{B}$ of ϵ^{fk} , and attach a linear head $h^l(\cdot)$ with parameters ψ to every block's output. This yields a multi-head D with the aim of distinguishing between $y \in Y$ and $x = G(z)$, $z \sim \mathcal{N}(0, I)$. The GAN losses, aggregated over heads by summation, are:

$$\mathcal{L}_{\text{GAN}}^G(\theta) = -\mathbb{E}_{t,z} \sum_{b \in \mathcal{B}} h^b(f^b(x_t)), \quad (8)$$

$$\begin{aligned} \mathcal{L}_{\text{GAN}}^D(\psi, \phi) = & \mathbb{E}_{t,y} \sum_{b \in \mathcal{B}} \max \left(0, 1 - h_{\psi}^b(f_{\phi}^b(y_t)) \right) \\ & + \mathbb{E}_{t,z} \sum_{b \in \mathcal{B}} \max \left(0, 1 + h_{\psi}^b(f_{\phi}^b(x_t)) \right). \end{aligned} \quad (9)$$

Attaching classifier heads after every encoder block enables D to contrast real vs. fake at both local and global scales, which is especially helpful in the few-shot regime $|Y| \leq 10$, mitigating overfitting and mode collapse.

3.6. Overall Training Objective

The **student**'s training update balances source preservation and target fitting via minimizing the dual-domain DMD and GAN generator losses:

$$\mathcal{L}_G(\theta) = \mathcal{L}_{\text{DMD}}^{\text{trg+src}}(\theta) + \lambda_{\text{GAN}}^G \mathcal{L}_{\text{GAN}}^G(\theta), \quad (10)$$

Algorithm 1: Uni-DAD Training Iteration

Input : Source teacher ϵ^{src} , Optional target teacher ϵ^{trg} , Target set $Y = \{y\}$, Weight factor a , Training step, Update ratio

Output: Student G (Adapted and Distilled)

```

1  $\epsilon^{\text{fk}} \leftarrow \epsilon^{\text{src}}$ 
2 if  $\epsilon^{\text{trg}} == \emptyset$  then
3    $\epsilon^{\text{trg}} \leftarrow \epsilon^{\text{src}}$ ; train_target  $\leftarrow \text{True}$ 
   // Prepare data
4  $t \sim \mathcal{U}\{0.02T, 0.98T\}$ 
5  $(z, \epsilon) \sim \mathcal{N}(0, I)$ 
6  $y_t \leftarrow q(y_t | y)$ ,  $y \sim Y$  // real
7  $x_t \leftarrow q(x_t | x)$ ,  $x \leftarrow G(z)$  // fake
   // Student
8 if step % ratio == 0 then
9    $\mathcal{L}_{\text{DMD}}^{\text{trg+src}} \leftarrow \text{DualDMD}(x_t, \epsilon, a)$  // Eq 5
10   $\mathcal{L}_{\text{GAN}}^G \leftarrow \text{MhGAN}(x_t)$  // Eq 8
11   $\mathcal{L}_G \leftarrow \mathcal{L}_{\text{DMD}}^{\text{trg+src}} + \lambda_{\text{GAN}}^G \mathcal{L}_{\text{GAN}}^G$  // Eq 10
12   $G \leftarrow \text{update}(G, \mathcal{L}_G)$ 
   // Fake Teacher & Discriminator
13  $\mathcal{L}_{\text{fk}} \leftarrow \text{MSE}(\epsilon^{\text{fk}}(\text{stop-grad}(x_t)), \epsilon)$  // Eq 6
14  $\mathcal{L}_{\text{GAN}}^D \leftarrow \text{MhGAN}(\text{stop-grad}(x_t), y_t)$  // Eq 9
15  $\mathcal{L}_{\text{fk+D}} \leftarrow \mathcal{L}_{\text{fk}} + \lambda_{\text{GAN}}^D \mathcal{L}_{\text{GAN}}^D$  // Eq 11
16  $\epsilon^{\text{fk}} \leftarrow \text{update}(\epsilon^{\text{fk}}, \mathcal{L}_{\text{fk+D}})$ 
   // Target Teacher
17 if step % ratio == 0 & train_target then
18    $\mathcal{L}_{\epsilon^{\text{trg}}} \leftarrow \text{MSE}(\epsilon^{\text{trg}}(y_t), \epsilon)$  // Eq 7
19    $\epsilon^{\text{trg}} \leftarrow \text{update}(\epsilon^{\text{trg}}, \mathcal{L}_{\text{trg}})$ 

```

where in practice, $\nabla_{\theta} \mathcal{L}_{\text{DMD}}^{\text{trg+src}}$ is used instead of $\mathcal{L}_{\text{DMD}}^{\text{trg+src}}(\theta)$ to update G 's parameters. The **fake teacher**'s training update combines its MSE and GAN discriminator losses:

$$\mathcal{L}_{\text{fk+D}}(\phi, \psi) = \mathcal{L}_{\text{fk}}(\phi) + \lambda_{\text{GAN}}^D \mathcal{L}_{\text{GAN}}^D(\psi, \phi). \quad (11)$$

The training of Uni-DAD involves alternating among minimizing three losses at each iteration: \mathcal{L}_G , $\mathcal{L}_{\text{fk+D}}$ and \mathcal{L}_{trg} (Alg. 1). In practice, the minimization for $\mathcal{L}_{\text{fk+D}}$ is performed 5-10 times [49] for each update of \mathcal{L}_G and \mathcal{L}_{trg} to allow ϵ^{fk} to keep up with the constantly changing output distribution of G .

4. Results and Discussion

4.1. Experimental Setup

Following the widely adopted FSIG benchmark [28, 51], we use the guided DDPM of Dhariwal and Nichol [8] pre-



Figure 5. Qualitative comparison for 10-shot adaptation from a guided DM [8] pretrained on FFHQ [17] to target domains of varying proximity to the source. Generated samples are randomly picked. Zoom in for details.

trained on the unconditional FFHQ dataset (70K images of diverse faces [17]²) as the source model, and adapt it to 10 pre-selected samples of four different target domains. We include two semantically closer domains: Babies [28] and Sunglasses [28], as well as two structurally distant domains: MetFaces [18] and AFHQ-Cat (Cats) [6]. We compare against recent DDPM-based FSIG methods, DDPM-PA [52] and CRDI [3], that use 1000-step DDPM and 25-

step DDIM samplers respectively. DDPM-PA provides no public code, and their results are limited to Babies and Sunglasses only. We quote their numbers when available without further verification. We implement three additional baselines: (i) FT, where we fine-tune the source DM on the target domain using the MSE loss (Eq. 1) and sample with 25 DDIM steps, (ii) DMD2-FT, where we first distill the DM via DMD2 [49], then fine-tune the resulting student on the target domain, and (iii) FT-DMD2, where we first fine-tune, and then distill via DMD2. To measure quality,

²Weights taken from <https://github.com/yandex-research/ddpm-segmentation>

Table 1. Comparison of $\text{FID} \downarrow$ and $\text{Intra-LPIPS} \uparrow$ across methods and 10-shot target domains. **Bold** indicates best result among *distilled* variants. Underline indicates best result among *all* models.

Variant	Method	NFE \downarrow	End-to-end	FID \downarrow			Intra-LPIPS \uparrow			
				Babies	Sunglasses	MetFaces	Cats	Babies	Sunglasses	MetFaces
<i>Non-distilled</i>	DDPM-PA [52]	1000	✓	48.92	34.75	—	—	<u>0.59</u>	<u>0.60</u>	—
	CRDI [3]	25	✓	48.52	24.62	121.36 [†]	220.95	0.52	0.50	0.41
	FT	25	✓	57.06	37.86	72.99	61.62	0.32	0.48	<u>0.45</u>
<i>Distilled</i>	DMD2-FT	3		140.27	77.49	129.26	89.32	0.08	0.20	0.08
	FT-DMD2	3		57.11	41.85	63.25	51.85	0.42	0.42	0.44
	Uni-DAD (no ϵ^{trg})	3	✓	47.38	22.57	72.18	199.91	0.45	0.51	0.42
	Uni-DAD	3	✓	45.09	24.45	58.13	55.32	0.46	0.54	0.36

[†] We were unable to reproduce CRDI’s reported FID of 94.86 [3]. However, our qualitative samples and Intra-LPIPS closely match their findings.

we report FID on 5K generated images per domain against held-out target sets ($|\text{Babies}|=2.5\text{K}$, $|\text{Sunglasses}|=2.7\text{K}$, $|\text{MetFaces}|=1.3\text{K}$, $|\text{Cats}|=5\text{K}$). We assess diversity via Intra-LPIPS [28] computed on 1K generations relative to the few-shot targets. All adaptations use 256×256 images. Training and hyperparameter details are provided in Appx.

4.2. Comparison with SoTA Methods

(a) Qualitative. Fig. 5 presents a qualitative comparison against baselines. Among *Non-distilled* variants, DDPM-PA exhibits reduced detail and noticeable color shifts. Despite no results for MetFaces and Cats, the authors’ report suggests limited adaptability when the domain shift goes beyond a simple style transfer (e.g., church \rightarrow landscape drawing) [52]. CRDI, being a non-training test-time procedure, struggles to move off the source manifold on distant domains. It frequently regenerates the same target exemplars with minor local variations, showing no attribute recombination and misaligned textures. FT suffers from inconsistent fitting, either leaking source-domain content (e.g., adults instead of babies, faces without sunglasses) or overfitting to a few target exemplars. Further, it exhibits color denaturation and lacks sharp details. Among *Distilled* variants, DMD2-FT naïvely nullifies the benefits of distillation, producing over-smoothed outputs with muted textures and limited diversity. FT-DMD2, benefits from the GAN in its DMD step, alleviating the inconsistent fitting of FT and producing relatively sharper images. However, it often overfits and regenerates the same target set samples. In contrast, Uni-DAD consistently yields sharp, high-quality, and diverse generations on both close and distant domains. It mitigates inconsistent fitting and composes attributes across the target set. Further, including the target teacher (ϵ^{trg}) allows stronger adaptation of structure to **distant domains** with slight diversity reduction.

(b) Quantitative. Tab. 1 displays a quantitative comparison. Compared to *Non-distilled* baselines, Uni-DAD consistently attains better FID, demonstrating higher-quality generation with only 3 denoising steps. Further, its Intra-

Table 2. Ablation of Uni-DAD components evaluated on $\text{FID} \downarrow$ (NFE = 3, 10-shot). Selected variants are in gray, with DMD^{trg} as an optional component. Mh: Multi-head, Sh: Single-head, B: Babies, M: MetFaces.

Group	Components				FID \downarrow	
	DMD ^{src}	DMD ^{trg}	GAN ^{Mh}	GAN ^{Sh}	B	M
<i>GAN_only</i>				✓	56.90	80.14
				✓	130.34	110.00
<i>DMD_only</i>		✓			110.39	68.05
	✓				166.99	105.67
	✓	✓			84.19	69.80
<i>DMD+GAN</i>		✓		✓	54.18	68.54
	✓			✓	57.58	83.67
	✓	✓		✓	48.89	80.24
			✓	✓	54.68	68.74
	✓		✓		47.38	64.13
	✓	✓	✓		45.09	58.13

LPIPS remains comparable to the *Non-distilled*, despite the well-known diversity reduction phenomenon caused by distillation [10]. Compared to *Distilled* variants, it consistently achieves stronger FID and Intra-LPIPS on **close domains**. This highlights the effectiveness of utilizing the source DMD for diversity preservation and distribution alignment. On distant domains, FT-based methods (FT-DMD2 and DMD2-FT) become generally more competitive. This is due to incompatible knowledge transfer in methods that promote source preservation (DDPM-PA, CRDI, Uni-DAD no ϵ^{trg}) [51]. By including the target teacher (ϵ^{trg}), our method achieves stronger FID compared to the FT-based methods, at the cost of a slight Intra-LPIPS degradation. This indicates the effectiveness of the target DMD for adapting structure in **distant domains**. Our results suggest the robustness of Uni-DAD to the size of domain shift, making it a versatile approach.

4.3. Ablations

(a) Qualitative Ablations. Fig. 3 illustrates the interplay between NFE and sample quality: higher NFE yields more detailed generation. However, this effect saturates at $NFE = 4$ with negligible visual gains beyond that. Fig. 4 ablates our dual-domain DMD’s weighting factor a (Eq. 2). When the target domain lies inside the source manifold (e.g., Babies), a lower value suffices for adaptation, whereas a higher value can facilitate adaptation to structurally dissimilar domains (e.g., MetFaces). In practice, too large a can cause target overfitting and make performance overly sensitive to the quality of the target teacher, whereas smaller values let the source term correct its imperfections. Our main results (Fig. 5 and Tab. 1) show that under mild domain shifts the target teacher (ϵ^{trg}) can be discarded altogether ($a = 0$). With larger shifts however, removing it can limit the student to style-transfer behavior.

(b) Component Analysis. Tab. 2 isolates the impact of the dual-domain DMD and the multi-head GAN on FID. While a single-head GAN outperforms our multi-head design when DMD is absent, the multi-head GAN becomes increasingly beneficial once paired with the DMD losses. The implication is that enforcing realism at multiple feature levels helps mitigate overfitting in few-shot contexts. Moreover, using DMD without the GAN often causes training instability and drift, which is mitigated by the target realism signals provided by the GAN. Overall, all components of our approach jointly improve generation quality.

(c) Available checkpoints. Tab. 3 ablates the effect of having different pre-trained checkpoints at the start of Uni-DAD training. In practice, one may have access to a distilled source model (*Pre-distilled G*), an adapted DM in the target domain (*Pre-adapted ϵ^{trg}*), or both. Uni-DAD is checkpoint-agnostic: an adapted DM’s weights can replace ϵ^{trg} with no online training needed, and a distilled source model can initialize the student. This makes Uni-DAD applicable both as an adaptation method for distilled models and as a distillation method for adapted models.

(d) Target Set Size and NFE. Tab. 4 ablates quantitative performance over $NFE \in \{1, 2, 3, 4\}$ in 1/5/10-shot settings. Increasing NFE improves FID up until $NFE = 3$, with little to no gain at $NFE = 4$. This highlights the effectiveness of our method as a few-step few-shot image generator. With $NFE = 3$, Uni-DAD consistently attains lower FID than CRDI in all settings, indicating its robustness across different few-shot regimes.

(e) Type of GAN loss. Tab. 5 ablates the choice of GAN loss. Among hinge [20], least-squares (LSGAN) [24], Wasserstein (WGAN) [1], and binary cross entropy (BCE) [11] losses, a simple BCE obtains the best FID with the multi-head GAN. Moreover, our multi-head GAN consistently outperforms a single-head counterpart, highlighting the importance of discriminating at multiple feature

Table 3. Available checkpoints at the start of Uni-DAD training and $FID \downarrow$ ($NFE = 3$). G is distilled via DMD2 [49] and ϵ^{trg} is adapted via fine-tuning. Selected variant for main results is in gray.

Available Checkpoints		$FID \downarrow$	
<i>Pre-distilled G</i>	<i>Pre-adapted ϵ^{trg}</i>	Babies	MetFaces
		45.09	58.13
✓		42.68	77.80
	✓	46.73	62.67
✓	✓	42.04	54.01

Table 4. Ablation on target set sizes and NFE, evaluated by $FID \downarrow$. B: Babies, M: MetFaces. **Bold** indicates best result. Selected variant for main results is in gray.

Methods	NFE \downarrow	1-shot		5-shot		10-shot	
		B	M	B	M	B	M
CRDI	25	105.51	145.10	51.71	126.34	48.52	121.36
Uni-DAD	4	72.38	95.44	45.86	81.85	41.39	59.49
Uni-DAD	3	90.33	90.29	52.73	83.69	45.09	58.13
Uni-DAD	2	95.69	114.78	68.75	98.36	62.45	79.08
Uni-DAD	1	109.55	132.79	93.52	103.84	98.52	89.03

Table 5. Ablation of GAN losses evaluated on $FID \downarrow$ ($NFE = 3$, 10-shot). **Bold** indicates best result. Selected variant for main results is in gray.

GAN Loss	Multi-head		Single-head	
	Babies	MetFaces	Babies	MetFaces
BCE	45.09	58.13	48.89	80.24
Hinge	45.82	64.83	50.92	72.11
LSGAN	46.18	91.55	47.98	64.36
WGAN	64.54	95.35	58.50	84.91

levels to avoid overfitting and increase stability.

5. Conclusion

We present Uni-DAD, a *single-stage* pipeline that unifies distillation and adaptation of DMs. It combines a dual-domain distribution-matching objective and a multi-head GAN. An optional target teacher can further improve adaptation to structurally distant domains. On FSIG benchmarks, it attains higher quality than recent adaptation methods with 25 steps, while requiring only ≤ 4 sampling steps. Further, it outperforms *two-stage* pipelines: *Adapt-then-Distill* and *Distill-then-Adapt* in quality and diversity. Our framework additionally provides a solution for adapting distilled models and distilling adapted ones. These results highlight a practical avenue for fast and high-quality image generation under scarce data and non-trivial domain shifts.

Limitations and Future Work: Incorporating a GAN increases hyperparameter sensitivity and can require care to

prevent overfitting. Moreover, Uni-DAD exhibits a trade-off between training and sampling cost: while it allows fast generation, it inherits the high computation cost of distillation. Future work includes automatic scheduling or learning of the DMD weighting and broader backbone generalization (e.g., SD-XL, video and audio DMs).

References

- [1] Martin Arjovsky, Soumith Chintala, and Léon Bottou. Wasserstein generative adversarial networks. In *International conference on machine learning*, pages 214–223. PMLR, 2017. 8
- [2] Yara Bahram, Mohammadhadi Shateri, and Eric Granger. Dogfit: Domain-guided fine-tuning for efficient transfer learning of diffusion models. In *Proceedings of the AAAI Conference on Artificial Intelligence*, 2026. 3, 1
- [3] Yu Cao and Shaogang Gong. Few-shot image generation by conditional relaxing diffusion inversion. In *European Conference on Computer Vision*, pages 20–37. Springer, 2024. 1, 2, 6, 7
- [4] Mathilde Caron, Hugo Touvron, Ishan Misra, Hervé Jégou, Julien Mairal, Piotr Bojanowski, and Armand Joulin. Emerging properties in self-supervised vision transformers. *arXiv preprint arXiv:2104.14294*, 2021. Submitted 29 Apr 2021; Revised 24 May 2021. 5
- [5] Clement Chadebec, Onur Tasar, Eyal Benaroche, and Benjamin Aubin. Flash diffusion: Accelerating any conditional diffusion model for few steps image generation. In *Proceedings of the AAAI Conference on Artificial Intelligence*, pages 15686–15695, 2025. 1, 2, 3, 5
- [6] Yunjey Choi, Youngjung Uh, Jaejun Yoo, and Jung-Woo Ha. Stargan v2: Diverse image synthesis for multiple domains. In *Proceedings of the IEEE/CVF conference on computer vision and pattern recognition*, pages 8188–8197, 2020. 6
- [7] Kamil Deja, Anna Kuzina, Tomasz Trzcinski, and Jakub Tomczak. On analyzing generative and denoising capabilities of diffusion-based deep generative models. *Advances in Neural Information Processing Systems*, 35:26218–26229, 2022. 1
- [8] Prafulla Dhariwal and Alexander Nichol. Diffusion models beat gans on image synthesis. *Advances in neural information processing systems*, 34:8780–8794, 2021. 1, 2, 5, 6
- [9] Rinon Gal, Yuval Alaluf, Yuval Atzmon, Or Patashnik, Amit H. Bermano, Gal Chechik, and Daniel Cohen-Or. An image is worth one word: Personalizing text-to-image generation using textual inversion. *arXiv preprint arXiv:2208.01618*, 2022. 1, 4
- [10] Rohit Gandikota and David Bau. Distilling diversity and control in diffusion models. *arXiv preprint arXiv:2503.10637*, 2025. 7
- [11] Ian J Goodfellow, Jean Pouget-Abadie, Mehdi Mirza, Bing Xu, David Warde-Farley, Sherjil Ozair, Aaron Courville, and Yoshua Bengio. Generative adversarial nets. *Advances in neural information processing systems*, 27, 2014. 8
- [12] Ligong Han, Yinxiao Li, Han Zhang, Peyman Milanfar, Dimitris Metaxas, and Feng Yang. Svdiff: Compact parameter space for diffusion fine-tuning. *arXiv preprint arXiv:2303.11305*, 2023. 5
- [13] Jonathan Ho and Tim Salimans. Classifier-free diffusion guidance. *arXiv preprint arXiv:2207.12598*, 2022. 3, 5
- [14] Jonathan Ho, Ajay Jain, and Pieter Abbeel. Denoising diffusion probabilistic models. *Advances in neural information processing systems*, 33:6840–6851, 2020. 1, 3
- [15] Yi-Ting Hsiao, Siavash Khodadadeh, Kevin Duarte, Wei-An Lin, Hui Qu, Mingi Kwon, and Rathesh Kalarot. Plug-and-play diffusion distillation. In *Proceedings of the IEEE/CVF Conference on Computer Vision and Pattern Recognition*, pages 13743–13752, 2024. 3
- [16] Edward Hu, Yelong Shen, Phillip Wallis, Zeyuan Allen-Zhu, Yuanzhi Li, Shean Wang, Lu Wang, and Weizhu Chen. Lora: Low-rank adaptation of large language models. *arXiv preprint arXiv:2106.09685*, 2021. 2
- [17] Tero Karras, Samuli Laine, and Timo Aila. A style-based generator architecture for generative adversarial networks. In *Proceedings of the IEEE/CVF conference on computer vision and pattern recognition*, pages 4401–4410, 2019. 6
- [18] Tero Karras, Miika Aittala, Janne Hellsten, Samuli Laine, Jaakko Lehtinen, and Timo Aila. Training generative adversarial networks with limited data. *Advances in neural information processing systems*, 33:12104–12114, 2020. 6
- [19] Nupur Kumari, Bingliang Zhang, Richard Zhang, Eli Shechtman, and Jun-Yan Zhu. Multi-concept customization of text-to-image diffusion. In *Proceedings of the IEEE/CVF Conference on Computer Vision and Pattern Recognition*, pages 19200–19210, 2023. 1, 4, 5
- [20] Jae Hyun Lim and Jong Chul Ye. Geometric gan. *arXiv preprint arXiv:1705.02894*, 2017. 8
- [21] Cheng Lu, Yuhao Zhou, Fan Bao, Jianfei Chen, Chongxuan Li, and Jun Zhu. Dpm-solver: A fast ode solver for diffusion probabilistic model sampling in around 10 steps. *Advances in neural information processing systems*, 35:5775–5787, 2022. 2
- [22] Simian Luo, Yiqin Tan, Longbo Huang, Jian Li, and Hang Zhao. Latent consistency models: Synthesizing high-resolution images with few-step inference. *arXiv preprint arXiv:2310.04378*, 2023. 2
- [23] Simian Luo, Yiqin Tan, Suraj Patil, Daniel Gu, Patrick von Platen, Apolinário Passos, Longbo Huang, Jian Li, and Hang Zhao. Lcm-lora: A universal stable-diffusion acceleration module. *arXiv preprint arXiv:2311.05556*, 2023. 3
- [24] Xudong Mao, Qing Li, Haoran Xie, Raymond YK Lau, Zhen Wang, and Stephen Paul Smolley. Least squares generative adversarial networks. In *Proceedings of the IEEE international conference on computer vision*, pages 2794–2802, 2017. 8
- [25] Kangfu Mei, Mauricio Delbracio, Hossein Talebi, Zhengzhong Tu, Vishal M Patel, and Peyman Milanfar. Codi: Conditional diffusion distillation for higher-fidelity and faster image generation. In *Proceedings of the IEEE/CVF Conference on Computer Vision and Pattern Recognition*, pages 9048–9058, 2024. 3
- [26] Chenlin Meng, Yutong He, Yang Song, Jiaming Song, Jiajun Wu, Jun-Yan Zhu, and Stefano Ermon. Sdedit: Guided

image synthesis and editing with stochastic differential equations. *arXiv preprint arXiv:2108.01073*, 2021. 1

[27] Zichen Miao, Zhengyuan Yang, Kevin Lin, Ze Wang, Zicheng Liu, Lijuan Wang, and Qiang Qiu. Tuning timestep-distilled diffusion model using pairwise sample optimization. *arXiv preprint arXiv:2410.03190*, 2024. 2, 3, 5

[28] Utkarsh Ojha, Yijun Li, Jingwan Lu, Alexei A Efros, Yong Jae Lee, Eli Shechtman, and Richard Zhang. Few-shot image generation via cross-domain correspondence. In *Proceedings of the IEEE/CVF conference on computer vision and pattern recognition*, pages 10743–10752, 2021. 2, 5, 6, 7

[29] Dustin Podell, Zion English, Kyle Lacey, Andreas Blattmann, Tim Dockhorn, Jonas Müller, Joe Penna, and Robin Rombach. Sdxl: Improving latent diffusion models for high-resolution image synthesis. *arXiv preprint arXiv:2307.01952*, 2023. 4, 3, 5

[30] Ben Poole, Ajay Jain, Jonathan T Barron, and Ben Mildenhall. Dreamfusion: Text-to-3d using 2d diffusion. *arXiv preprint arXiv:2209.14988*, 2022. 4

[31] Alec Radford, Jong Wook Kim, Chris Hallacy, Aditya Ramesh, Gabriel Goh, Sandhini Agarwal, Girish Sastry, Amanda Askell, Pamela Mishkin, Jack Clark, Gretchen Krueger, and Ilya Sutskever. Learning transferable visual models from natural language supervision. *arXiv preprint arXiv:2103.00020*, 2021. Version v1. 5

[32] Shwetha Ram, Tal Neiman, Qianli Feng, Andrew M. Stuart, Son Tran, and Trishul A. Chilimbi. Dreamblend: Advancing personalized fine-tuning of text-to-image diffusion models. In *Proceedings of the Winter Conference on Applications of Computer Vision (WACV)*, pages 3614–3623, 2025. 5

[33] Google Research. dreambooth: Fine-tuning text-to-image diffusion models for subject-driven generation (github repository). <https://github.com/google/dreambooth>, 2023. Archived: May 9, 2024; CC-BY-4.0 license. 5

[34] Robin Rombach, Andreas Blattmann, Dominik Lorenz, Patrick Esser, and Björn Ommer. High-resolution image synthesis with latent diffusion models. In *Proceedings of the IEEE/CVF conference on computer vision and pattern recognition*, pages 10684–10695, 2022. 1, 4, 3, 5

[35] Nataniel Ruiz, Yuanzhen Li, Varun Jampani, Yael Pritch, Michael Rubinstein, and Kfir Aberman. Dreambooth: Fine tuning text-to-image diffusion models for subject-driven generation. *arXiv preprint arXiv:2208.12242*, 2023. 1, 2, 3, 4, 5

[36] Chitwan Saharia, William Chan, Saurabh Saxena, Lala Li, Jay Whang, Emily Denton, Seyed Kamyar Seyed Ghasemipour, Burcu Karagol Ayan, S. Sara Mahdavi, Rapha Gontijo Lopes, Tim Salimans, Jonathan Ho, David J Fleet, and Mohammad Norouzi. Photorealistic text-to-image diffusion models with deep language understanding. <https://arxiv.org/abs/2205.11487>, 2022. arXiv:2205.11487. 1

[37] Tim Salimans and Jonathan Ho. Progressive distillation for fast sampling of diffusion models. *arXiv preprint arXiv:2202.00512*, 2022. 1, 2

[38] Axel Sauer, Frederic Boesel, Tim Dockhorn, Andreas Blattmann, Patrick Esser, and Robin Rombach. Fast high-resolution image synthesis with latent adversarial diffusion distillation. In *SIGGRAPH Asia 2024 Conference Papers*, pages 1–11, 2024. 2

[39] Axel Sauer, Dominik Lorenz, Andreas Blattmann, and Robin Rombach. Adversarial diffusion distillation. In *European Conference on Computer Vision*, pages 87–103. Springer, 2024. 2

[40] Christoph Schuhmann, Romain Beaumont, Richard Vencu, Cade Gordon, Ross Wightman, Mehdi Cherti, Theo Coombes, Aarush Katta, Clayton Mullis, Mitchell Wortsman, et al. Laion-5b: An open large-scale dataset for training next generation image-text models. *Advances in neural information processing systems*, 35:25278–25294, 2022. 5

[41] Jascha Sohl-Dickstein, Eric Weiss, Niru Maheswaranathan, and Surya Ganguli. Deep unsupervised learning using nonequilibrium thermodynamics. In *International conference on machine learning*, pages 2256–2265. pmlr, 2015. 1, 3

[42] Jiaming Song, Chenlin Meng, and Stefano Ermon. Denoising diffusion implicit models. *arXiv preprint arXiv:2010.02502*, 2020. 2

[43] Yang Song, Jascha Sohl-Dickstein, Diederik P Kingma, Abhishek Kumar, Stefano Ermon, and Ben Poole. Score-based generative modeling through stochastic differential equations. *arXiv preprint arXiv:2011.13456*, 2020. 1, 3, 4

[44] Yang Song, Prafulla Dhariwal, Mark Chen, and Ilya Sutskever. Consistency models. In *International Conference on Machine Learning*, pages 32211–32252. PMLR, 2023. 1, 2

[45] Xiyu Wang, Baijiong Lin, Daochang Liu, Ying-Cong Chen, and Chang Xu. Bridging data gaps in diffusion models with adversarial noise-based transfer learning. In *Forty-first International Conference on Machine Learning*, 2024. 3

[46] Yuxiang Wei, Yabo Zhang, Zhilong Ji, Jinfeng Bai, Lei Zhang, and Wangmeng Zuo. Elite: Encoding visual concepts into textual embeddings for customized text-to-image generation. *arXiv preprint arXiv:2302.13848*, 2023. 5

[47] Ceyuan Yang, Yujun Shen, Zhiyi Zhang, Yinghao Xu, Jia-peng Zhu, Zhirong Wu, and Bolei Zhou. One-shot generative domain adaptation. In *Proceedings of the ieee/cvf international conference on computer vision*, pages 7733–7742, 2023. 2

[48] Yunzhi Yao, Shaohan Huang, Wenhui Wang, Li Dong, and Furu Wei. Adapt-and-distill: Developing small, fast and effective pretrained language models for domains. In *Findings of the Association for Computational Linguistics: ACL-IJCNLP 2021*, pages 460–470, 2021. 3

[49] Tianwei Yin, Michaël Gharbi, Taesung Park, Richard Zhang, Eli Shechtman, Fredo Durand, and Bill Freeman. Improved distribution matching distillation for fast image synthesis. *Advances in neural information processing systems*, 37:47455–47487, 2024. 1, 2, 3, 4, 5, 6, 8

[50] Tianwei Yin, Michaël Gharbi, Richard Zhang, Eli Shechtman, Fredo Durand, William T Freeman, and Taesung Park. One-step diffusion with distribution matching distillation. In

Proceedings of the IEEE/CVF conference on computer vision and pattern recognition, pages 6613–6623, 2024. [1](#), [2](#), [4](#)

- [51] Yunqing Zhao, Chao Du, Milad Abdollahzadeh, Tianyu Pang, Min Lin, Shuicheng Yan, and Ngai-Man Cheung. Exploring incompatible knowledge transfer in few-shot image generation. In *Proceedings of the IEEE/CVF Conference on Computer Vision and Pattern Recognition*, pages 7380–7391, 2023. [2](#), [5](#), [7](#)
- [52] Jingyuan Zhu, Huimin Ma, Jiansheng Chen, and Jian Yuan. Few-shot image generation with diffusion models. *arXiv preprint arXiv:2211.03264*, 2022. [1](#), [2](#), [6](#), [7](#)



Uni-DAD: Unified Distillation and Adaptation of Diffusion Models for Few-step Few-shot Image Generation

Supplementary Material

Table of Contents

6 Proposed Method Contd.	1
7 Results and Discussion Contd.	1
7.1 Training Details.....	1
7.2 Uni-DAD in Style Transfer.....	2
7.3 Computational Cost Analysis.....	2
8 Subject-driven Personalization	3
8.1 Overview	3
8.2 Related Work	4
8.3 Adapting Uni-DAD to SDP	5
8.4 Experimental setup	5
8.5 Training Details	5
8.6 Results and Discussion	6

6. Proposed Method Contd.

Why a source score is useful. The source teacher ϵ^{src} , trained on large and diverse data, can be viewed as a general image-manifold approximator [2]. Moreover, it has been shown that diffusion models operating in noisy space can generalize across distributions and denoise out-of-domain inputs [7, 26]. Consequently, ϵ^{src} offers a stable score around x_t that regularizes \mathcal{G} and helps preserve general information shared between the source and target domains.

7. Results and Discussion Contd.

7.1. Training Details

Selected images for the k -shot ablation. Figure 6 shows representative training images for ablating the number of shots $k \in \{1, 5, 10\}$ per target domain in Table.

Global Details. We include details of Uni-DAD, DMD2-FT, and CRDI [3]. All models are trained with image size 256×256 and each dataset is resized from 1024×1024 to this resolution for training. Since the Inception network expects 299×299 input images for FID calculation, following common practice, we adopt the $1024 \rightarrow 256 \rightarrow 299$ resizing pipeline for consistency of evaluation with prior work [3]. We report the best FID³ observed during training over 20K iterations and its corresponding Intra-LPIPS⁴.

Uni-DAD Training. Training is conducted over one 80GB H100 GPU for 2 to 3 hours [6]. When using e^{trg} , We set $a = 0.25$ for close domains (Babies, Sunglasses), and

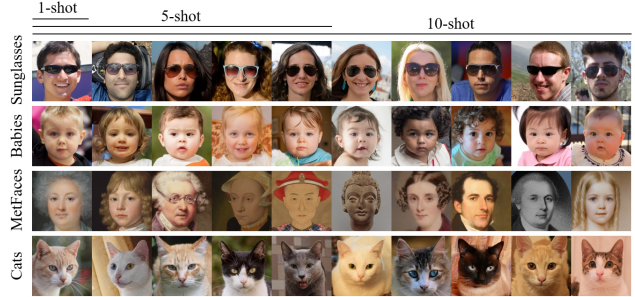


Figure 6. Representative target sets used in our experiments. Rows: domains. Column groups: k -shot setting ($k \in \{1, 5, 10\}$).

$a = 0.75$ for distant ones (MetFaces, Cats). Furthermore, we set $\lambda_{\text{GAN}}^G = 0.01$ and $\lambda_{\text{GAN}}^D = 0.03$ for all experiments. All experiments are performed with $\text{NFE} = 3$ unless specified otherwise. The generator update ratio is set to 5. For the multi-head GAN discriminator, for each feature map of dimension $C \times H \times W$, we apply a single 1×1 convolution to project the C channels to a single-channel map, followed by a global average pooling to obtain a scalar logit. This directly aggregates information from multiple resolutions. For the single-head GAN classifier, we use a deep bottleneck branch based on DMD2 [49]. We use a batch size of one, mixed-precision (bf16), and random horizontal flipping augmentation. The learning rate is $2e^{-6}$ for all models.

DMD2-FT Training. The DMD2 distilled model generates FFHQ-aligned images and attains FID@5k of 24.80. For fine-tuning the distilled model, we test two possible design choices of training-time time-step sampling: (i) Only sampling time-steps based on NFE (e.g., $\text{NFE} = 3$, $t \in \{333, 666, 1000\}$), and (ii) Sampling from the whole possible steps $T \in \{1, \dots, 1000\}$. We observe similar behavior in both cases and choose the first option. We use a batch size of one, mixed-precision (bf16), and random horizontal flipping augmentation. The learning rate is $2e^{-6}$ for both stages. FT-DMD2 follows the same hyperparameter configuration as DMD2-FT.

CRDI Training. We train CRDI [3] using the authors' released code and configurations⁵. We use four A100 GPUs to match their batch size of 10 and train for roughly 1 GPU hour. On closer domains (Sunglasses and Babies), follow-

³FID code taken from <https://github.com/bioinf-jku/TTUR>

⁴Intra-LPIPS code taken from <https://github.com/YuCao16/CRDI>

⁵CRDI code taken from <https://github.com/YuCao16/CRDI>



Figure 7. Style transferred images generated by Uni-DAD.

Variant	Method	Training cost (20K iters, †: not applicable)			Test cost (5K generations, batch size 10)			
		GPU · h	GPU	Mem [GB]	Time [m]	Mem [GB]	TFLOPs/img	NFE
<i>Non-distilled</i>	CRDI †	1	4 A100	124.7	63	14	55.7	25
	FT	0.8	1 H100	27.6	35	14	55.7	25
<i>Distilled</i>	FT-DMD2	3	1 H100	40.4	4.2	13	2.2	3
	DMD2-FT	3	1 H100	40.4	4.2	13	2.2	3
	Uni-DAD (No ϵ^{trg})	2.2	1 H100	40.3	4.2	13	2.2	3
	Uni-DAD	2.8	1 H100	48.8	4.2	13	2.2	3

Table 6. Training and test-time computational cost comparison. Mem: memory. h: hour, m: minute.

ing the authors’ guidance, we set $t_{\text{start}} = 5$, $t_{\text{end}} = 20$, and $\text{num_gradient} = 15$. On MetFaces, we use $t_{\text{start}} = 5$, $t_{\text{end}} = 15$, and $\text{num_gradient} = 10$ as suggested. However, the FID that we attain in this case is different what they report. We include both our results and theirs. On Cats, we adopt the same configuration as MetFaces.

7.2. Uni-DAD in Style Transfer

Our method can also be utilized as a one-shot style transfer technique, without requiring a target teacher (ϵ^{trg}). As an example, we transfer and distill the FFHQ source model using the style of “*The Starry Night*” by *Vincent van Gogh*. As shown in Fig. 7, Uni-DAD successfully transfers the artistic style while preserving underlying facial structures and diversity in generation. This suggests that, as long as the target domain does not require structural changes and differs primarily in styles, Uni-DAD can adapt using only the GAN branch, while DMD^{src} enforces consistency with the original source distribution. Babies and Sunglasses are two such cases, as they correspond to subsets of the broader FFHQ distribution.

7.3. Computational Cost Analysis

Tab. 6 compares training and test-time costs across adaptation pipelines. The *Non-distilled* methods, CRDI and FT, have low training budgets of 1 and 0.8 GPU·hs, respectively, but both rely on long denoising trajectories (NFE= 25) at

test time. As a result, they incur a high per-image cost of ≈ 55.7 TFLOPs and require about 35 minutes to generate 5K samples on a single H100 GPU. By contrast, *Distilled* methods greatly reduce the test-time cost: they use only ≈ 6.6 TFLOPs per image with NFE= 3, and need just 4.2 minutes for the same 5K-sample generation task, yielding roughly a $8.3\times$ reduction in sampling time and TFLOPs per image. This efficient inference comes at the price of additional distillation compute. The two-stage pipelines (FT-DMD2 and DMD2-FT) require a FT stage of 0.8 GPU · hs and 27.6 GB memory, and a DMD2 distillation stage of 2.2 GPU · h and 40.4 GB memory, for a total of 3 GPU · h and a peak training memory of 40.4 GB per method. Our proposed Uni-DAD attains the same fast sampler while keeping the training cost lower: without a target teacher (no ϵ^{trg}), it uses a single-stage 2.2 GPU · h schedule, and the full Uni-DAD with a target teacher increases this only to 2.8 GPU · h, still below the two-stage baselines. The target-teacher variant raises peak memory from ≈ 40 GB to 48.8 GB (about 21% higher), but remains comfortably within the capacity of a single H100 GPU. Overall, Uni-DAD introduces only a modest one-time training overhead while delivering a highly efficient 3-step sampler at test time. Designing more parameter-efficient variants of Uni-DAD is an exciting direction for future work.



Figure 8. Additional samples from Uni-DAD **without** ϵ^{trg} ($a = 0$ for all domains).

7.4. Additional Generated Samples

Figs. 8 and 9 show 100 additional samples generated by Uni-DAD on Babies, Sunglasses, MetFaces, and Cats, without and with target teacher ϵ^{trg} included, respectively. Without ϵ^{trg} , the model fully adapts to close domains (Babies and Sunglasses), and adapts to the style of the distant target domains (MetFaces and Cats). The inclusion of the target teacher allows higher fidelity to the structure of the

distant domains, at the cost of slight diversity reduction.

8. Subject-driven Personalization

8.1. Overview

We further extend Uni-DAD beyond FSIG and apply it to conditional text-to-image diffusion models [29, 34]. In this setting, the goal is subject-driven personalization (SDP) [35], where the model must learn a new subject iden-

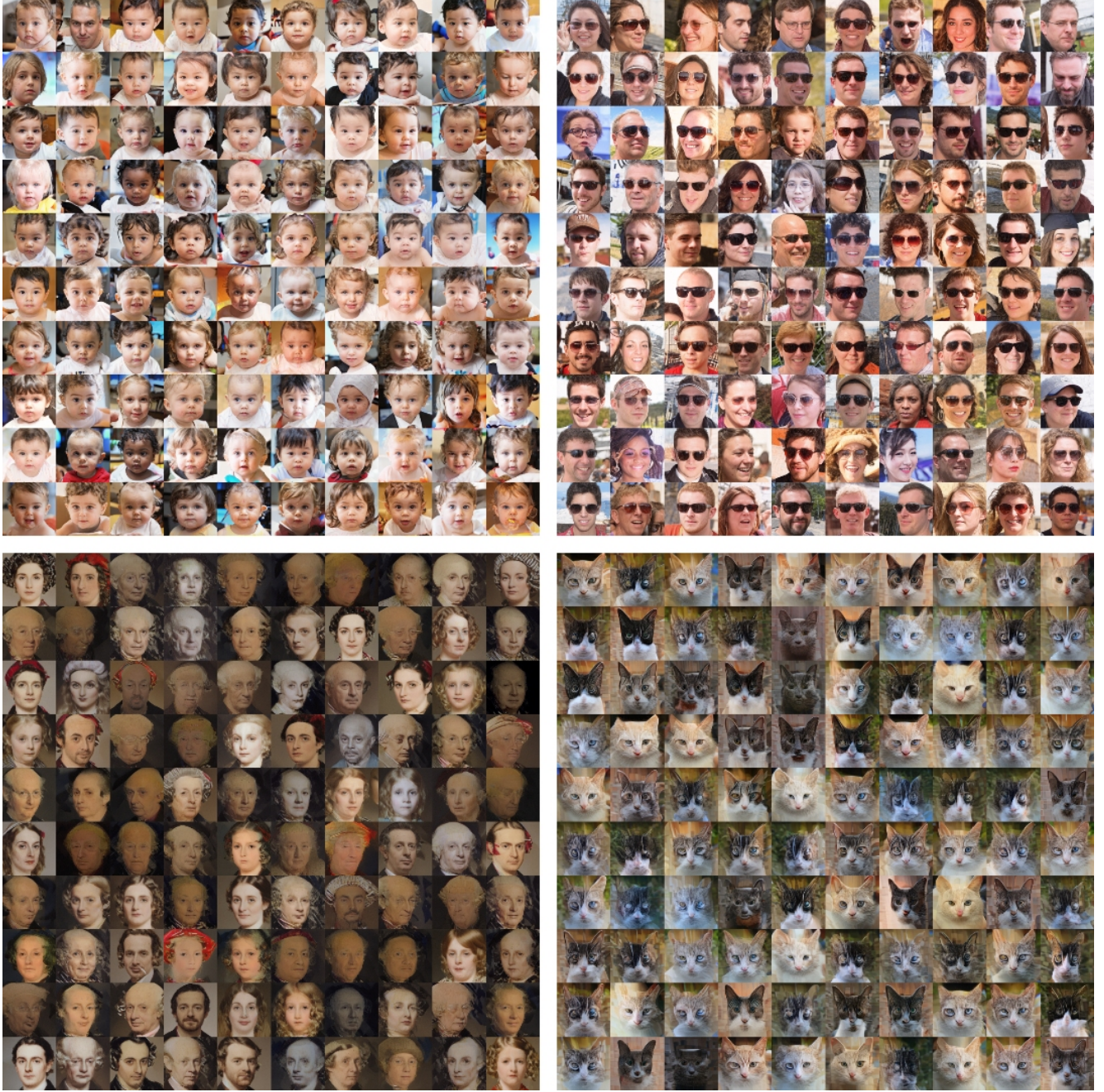


Figure 9. Additional samples from Uni-DAD with ϵ^{trg} ($\alpha = 0.25$ for Babies/Sunglasses and $\alpha = 0.75$ for MetFaces/Cats).

ity from only a handful of images and reproduce it faithfully across diverse textual prompts. SDP remains computationally expensive due to the slow sampling of adapted diffusion models. Here, we show that Uni-DAD provides an efficient and high-quality personalization pipeline while requiring only **one** sampling step at test time.

8.2. Related Work

SDP approaches can be broadly grouped into token-based and fine-tuning-based methods. Token-based approaches such as Textual Inversion [9] learn a subject embedding tied to a rare token, whereas DreamBooth [35] fine-tunes the DM on the subject images with a unique identifier. Custom Diffusion [19] adapts cross-attention layers to support multiple subjects in the same image. More recent work

focuses on parameter-efficient personalization, including SVDiff [12] and ELITE [46], which lower training cost but do not reduce the inherently slow sampling of diffusion models. In contrast, Uni-DAD addresses the sampling bottleneck by providing a one-stage personalization pipeline that both adapts and distills the model, enabling fast and high-quality subject-driven generation with only one denoising step.

8.3. Adapting Uni-DAD to SDP

Conditioning on Subject Prompts: SDP requires conditioning the DM on textual prompts that specify the subject identity. Uni-DAD naturally extends to this setting by incorporating prompt information into all conditional score evaluations. Let c denote the *instance prompt*, typically formatted as “a [rare token] [class noun]”, where the rare token uniquely identifies the subject (from 4–6 example images) and the class noun specifies the broader semantic category (e.g., “dog”, “cat”, “vase”). This prompt is provided to the models that undergo learning, i.e., the student generator G , the fake teacher ϵ^{fk} , and the target teacher ϵ^{trg} . Injecting c ensures that these models associate the rare token with the subject identity being learned.

Class-Prior Prompts: To maintain generality and prevent overfitting, we additionally define a *class-prior prompt* $c^{\text{prior}} = “a [class noun]”$, which is fed to the frozen source teacher ϵ^{src} . Since ϵ^{src} has not been trained on the specific subject, c^{prior} enables it to produce class-consistent but subject-agnostic guidance. This separation of prompts is crucial: ϵ^{src} continues to act as a diversity-inducing regularizer, stabilizing identity learning by preserving shared class-level structure.

Uni-DAD Components: All components of Uni-DAD (i.e., dual-domain DMD, fake and target teachers, and the multi-head GAN) operate unchanged except for the inclusion of prompt conditioning at each time-step. The dual-domain DMD now aligns conditional distributions, guiding the student to preserve general class semantics (via $\epsilon^{\text{src}}(\cdot | c^{\text{prior}})$) while adapting to the personalized subject (via $\epsilon^{\text{trg}}(\cdot | c)$). Likewise, the GAN discriminator receives c to encourage realistic subject-specific details at multiple feature scales.

8.4. Experimental Setup

Following the standard DreamBooth benchmark [35], we use Stable Diffusion v1.5 (SDv1.5) [34], pretrained on LAION-5B [40], as the source model. We evaluate on three representative instances from the DreamBooth dataset: *cat2*, *dog6*, and *vase*. Each subject is represented by 4–6 images taken from the DreamBooth dataset [33]. The full DreamBooth dataset contains 30 distinct subjects (9 humans and 21 objects). For each target instance, we generate 100 personalized samples (25 prompts \times 4 seeds), follow-

ing the prompt templates from DreamBooth covering recontextualization and accessorization. Prompt sets differ for objects (*vase*) and live subjects (*cat2*, *dog6*).

Baselines. We compare Uni-DAD against: (i) *non-distilled* DreamBooth [35] using 50-step DDIM sampling totaling $\text{NFE} = 2 \times 50$ for sampling with classifier-free guidance [13], (ii) *distilled* PSO [27], which fine-tunes a Turbo-distilled model [5] on an SDXL backbone [29] and samples with 4 steps ($\text{NFE} = 4$, and (iii) two-stage *distilled* DMD2-DreamBooth, where we fine-tune a DMD2-distilled SDv1.5 backbone [49] using the DreamBooth objective. Since PSO provides only SDXL code, our comparison adopts the SDXL-resolution results reported by the authors [27]. This introduces a resolution and backbone mismatch (1024×1024 instead of 512×512 and SDXL instead of SDv1.5) but is the fairest available comparison.

Evaluation Metrics. Following [35], identity preservation is measured using DINO (ViT-S/16) similarity [4] and CLIP-I (ViT-B/32) cosine similarity. Text–image alignment is quantified using CLIP-T (ViT-B/32) [31]. All models are evaluated at 512×512 resolution except PSO. Uni-DAD uses a single denoising step ($\text{NFE}=1$), enabling significantly faster sampling compared to the multi-step baselines, PSO, and DreamBooth.

8.5. Training Details

Uni-DAD Training. All models are trained with a learning rate of 5×10^{-6} . The multi-head GAN uses discriminator and generator weights of $\lambda_{\text{GAN}}^D = 0.01$ and $\lambda_{\text{GAN}}^G = 0.001$, respectively. The update ratio for G and ϵ^{trg} is set to 10. The student generator G is initialized from the DMD2 pre-distilled SDv1.5 weights⁶. We set the DMD weighting factor to $a = 0.75$, matching the distant-domain configuration used for FSIG. Uni-DAD is trained for 5k iterations on a single H100 GPU (≈ 50 GB memory usage), with best generations typically appearing between 4k–5k steps. Training time is ≈ 1.6 hour per subject.

DreamBooth Training. For the DreamBooth baseline, we follow prior preservation training by generating 1,000 samples of the form “a [class noun]” using SDv1.5. We fine-tune for 800 iterations per instance, using a batch size of 1 and a fixed learning rate of 5×10^{-6} . DreamBooth commonly uses 400–1,200 steps depending on the subject [19, 27, 32, 46]. we find 800 steps of training to be sufficient in reproducing the authors’ reported quality across subjects.

DMD2-DreamBooth Training. To construct this two-stage *distilled* baseline, we initialize the DreamBooth pipeline using DMD2 SDv1.5 checkpoints and fine-tune the student with the standard DreamBooth objective. We perform one-step sampling following DMD2-distilled generation.

⁶Weights taken from <https://github.com/tianweiy/DMD2>

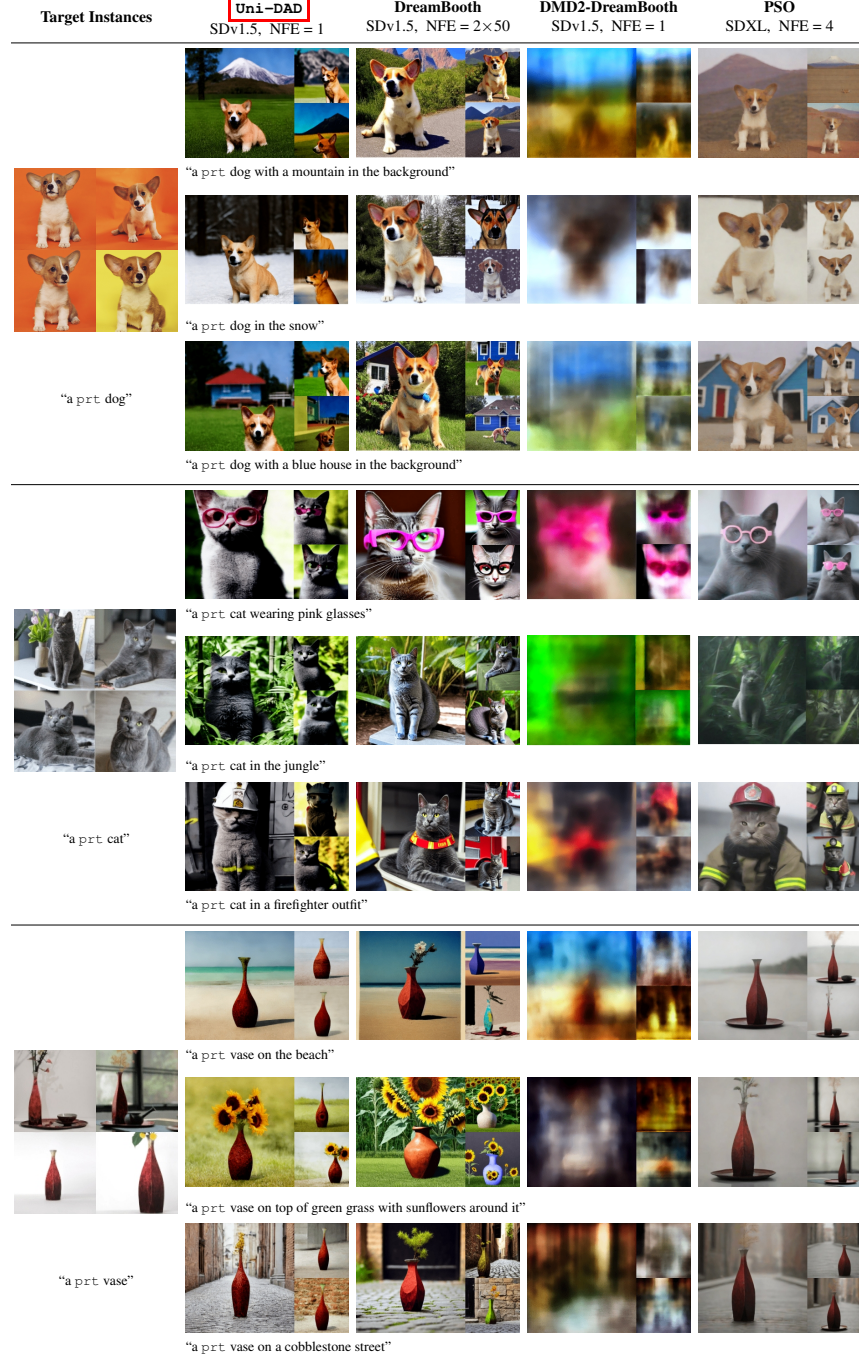


Figure 10. Qualitative comparison for personalization to the three instances (dog6, cat2, vase).

PSO Training. PSO operates on the SDXL-Turbo backbone and samples using 4 denoising steps.⁷ We use the official training setup for each subject. All models are evaluated after 800 training steps.

⁷https://github.com/ZichenMiao/Pairwise_Sample_Optimization

8.6. Results and Discussion

Fig. 10 shows a qualitative comparison across three subjects (dog6, cat2, vase). Across all subjects, Uni-DAD consistently produces sharp and identity-faithful generations with strong prompt alignment, despite using only a single denoising step (NFE = 1). In contrast, DreamBooth,

Table 7. Comparison across three personalization instances (dog6, cat2, vase) using DINO (D), CLIP-I (C-I), and CLIP-T (C-T) metrics \uparrow .

Variant	Method	NFE \downarrow	Backbone	dog6			cat2			vase			Average		
				D	C-I	C-T	D	C-I	C-T	D	C-I	C-T	D	C-I	C-T
<i>Non-distilled</i>	DreamBooth	2×50	SDv1.5	0.642	0.809	0.300	0.695	0.826	0.301	0.499	0.738	0.335	0.612	0.791	0.312
	PSO	4	SDXL	0.835	0.860	0.288	0.627	0.768	0.333	0.671	0.822	0.310	0.711	0.817	0.310
<i>Distilled</i>	DMD2-DreamBooth	1	SDv1.5	0.110	0.565	0.257	0.196	0.592	0.261	0.232	0.632	0.260	0.179	0.596	0.259
	Uni-DAD	1	SDv1.5	0.665	0.785	0.261	0.584	0.762	0.280	0.644	0.765	0.273	0.631	0.771	0.271

with $\text{NFE} = 2 \times 50$ often exhibits identity drift or introduces unintended stylistic artifacts. The two-stage DMD2-DreamBooth baseline is fast with $\text{NFE} = 1$, but suffers from severe over-smoothing and loss of detail. This further confirms that *Distill-then-Adapt* under the original diffusion loss degrades personalization quality. PSO achieves reasonable text alignment and preserves identity in some cases, but frequently produces over-smoothed or "plasticky" textures. This occurs even though PSO operates with the stronger SDXL backbone at a higher resolution (1024×1024) and uses more denoising steps ($\text{NFE} = 4$), making the comparison inherently biased in its favor. Among the SDv1.5-based methods, Uni-DAD stands out: it maintains prompt fidelity and subject-specific structure under challenging viewpoint and background changes, demonstrating robust generalization despite its extreme sampling efficiency.

Tab. 7 introduces a quantitative comparison of Uni-DAD with the SDP baselines. Despite operating under a rigid 1-step sampling regime, Uni-DAD achieves CLIP-based identity and text-image similarity scores that approach those of multi-step DreamBooth, while substantially outperforming its 1-step distilled counterpart, DMD2-DreamBooth. These results highlight the effectiveness of Uni-DAD as an efficient fast sampler for subject-driven personalization.